Atmospheric Environment 69 (2013) 325–333

Contents lists available at SciVerse ScienceDirect

Atmospheric Environment

journal homepage: www.elsevier.com/locate/atmosenv

Collection efficiency and interstage loss of nanoparticles in micro-orifice-based cascade impactors

Chun-Nan Liu, Amit Awasthi, Yi-Hung Hung, Chuen-Jinn Tsai*

Institute of Environmental Engineering, National Chiao Tung University, No. 1001, University Road, Hsinchu 30010, Taiwan

HIGHLIGHTS

- ► Nanoparticle loss occurs in lower stages of the micro-orifice cascade impactors.
- ► Nozzle plates with step-shape nozzle results in possible nozzle clogging.
- ► New NMCI with nozzles of smooth nozzle shape prevents nozzle clogging.
- ► New NMCI can facilitate accurate mass size distribution measurement of aerosols.

ARTICLE INFO

Article history:
Received 17 September 2012
Received in revised form
3 December 2012
Accepted 4 December 2012

Keywords:
Nanoparticle
Cascade impactor
Particle loss

ABSTRACT

In this study, two micro-orifice-based cascade impactors, including the micro-orifice uniform deposit impactor (MOUDI, MSP Model 110) and the NCTU micro-orifice cascade impactor (NMCI), were tested for the collection efficiency and interstage loss of nanoparticles. In the NMCI, new nozzle plates with smooth nozzle shape made by the LIGA (Lithography, Electroplating, and Molding) process were used to replace the 7th–10th stages in one of the MOUDI. Test results show that after adjusting proper S/W ratios (S: jet to plate distance, W: nozzle diameter) to 2.52, 3.01, 13.44, and 24.75 for the 7th, 8th, 9th and 10th stage of the NMCI, respectively, and 5.56, 11.18, 9.3, and 10.9 for the 7th, 8th, 9th and 10th stage of the MOUDI, respectively, the cutoff aerodynamic diameters (d_{pa50}) are close to the nominal values given in Marple et al. (1991). Different S/W ratios are needed due to differences in the nozzle shape and nozzle diameter between two cascade impactors. Total interstage loss of nanoparticles from the inlet to the 6th–10th stage of the MOUDI exists due to the convection-diffusion mechanism, which increases with decreasing d_{pa}. For the MOUDI, total loss is 2.9–15.3 % (d_{pa}: 105.8 to 15.4 nm) for the inlet to the 6th stage and it increases to 20.1–26.1 % (d_{pa}: 23 to 15.4 nm) for the inlet to the 10th stage, respectively. Similar but slightly lower loss also exists in the NMCI. Field comparison tests in the ambient air show that mass size distributions measured by the MOUDI agree well with those of the NMCI. Finally, nozzle clogging tests using high concentration incense smokes indicate that the NMCI has a much less tendency for particles to clog in the nozzles than the MODUI.

1. Introduction

Cascade impactors are used to measure aerosol mass size distributions and the collected samples can further be analyzed for chemical compositions (Chen et al., 2010; Kim et al., 2012; Kudo et al., 2012; Wang et al., 2010; Zhu et al., 2010, 2012). Traditionally, the smallest cutoff aerodynamic diameter (d_{pa50}) of a cascade impactor is around 0.5 μm, which leads to a poor size resolution of submicron particles and nanoparticles. To obtain a lower d_{pa50}, improved cascade impactors have been developed, such as the micro-orifice uniform deposit impactor (MOUDI) (Marple et al., 1991), the low pressure impactor (LPI) (Hering et al., 1979) and the electric low pressure impactor (ELPI) (Keskinen et al., 1992). Among them, the MOUDI is the most widely used device (Chow and Watson, 2007) because of its relatively smaller interstage pressure drop as compared to low pressure impactors which reduces potential evaporation of volatile aerosol species. Recently, a novel inertial filter was also developed and equipped at downstream of a four stages cascade impactor for classifying nanoparticles with much lower pressure drop to avoid more loss of volatile components (Otani et al., 2007; Furuuchi et al., 2010).

There are three major concerns when using cascade impactors: solid particle bounce, overloading of collected particles on the

* Corresponding author. Tel.: +886 35731880; fax: +886 35727835.
E-mail address: cjtsai@mail.nctu.edu.tw (C.-J. Tsai).

1352-2310/$ – see front matter © 2012 Elsevier Ltd. All rights reserved.
http://dx.doi.org/10.1016/j.atmosenv.2012.12.003

impaction plate and interstage loss (Marple et al., 2001). Many efforts have been made to resolve these problems. For example, different types of impaction substrates such as oil-coated substrates (Turner and Hering, 1987; Pak et al., 1992; Peters et al., 2001; Liu et al., 2011; Tsai et al., 2012), porous substrates (Huang et al., 2005, 2001) and specially designed substrates (Chang et al., 1999; Tsai and Cheng, 1995) were used to reduce solid particle bounce. In case that uncoated substrates are needed to avoid interference with chemical analysis of collected samples, Chen et al. (2011) suggested to condition the relative humidity (RH) of the incoming aerosols of the MOUDI to be higher than 75 or 65%, respectively, for uncoated aluminum foil or Teflon filter substrates. Similar conclusion was also found in Vasiliou et al. (1999). For increasing the particle loading capacity on impaction substrates, rotating substrates (Marple et al., 1991; Tsai et al., 2012), oil-soaked Teflon filters (Turner and Hering, 1987; Tsai et al., 2012) and impaction plates of special designs (Tsai and Cheng, 1995) provide possible solutions.

Besides collection efficiency, interstage loss data are also critical to complete the calibration of a cascade impactor since it may result in the shift of the collection efficiency curve to the smaller particle size (Liu et al., 2011) or even lift the left tail end of the curve (Hillamo and Kauppinen, 1991). The interstage loss in the MOUDI was measured during its initial development (Marple et al., 1991). However, the loss for nanoparticles with the diameter smaller than the d_{pa50} of each of the lower stages was not tested. In addition, the loss of nanoparticle can occur in the upstream stages before a certain lower stage, which is hard to measure because the loss per stage is small unless the test is conducted from the inlet to a specific lower stage. In Virtanen et al. (2001), particles with the size from 10 to 400 nm were used to measure the loss for the 5th to 12th stage of the ELPI with the corresponding d_{pa50} ranging from 260 nm to 6.7 μm. However, only particles (silver particles: 10–40 nm, DOS particles: 40–400 nm) which were smaller than d_{pa50} and deposited on the impaction plates of the stages were considered as particle loss while particles might also deposit between stages. In addition, particle loss in the lower 1st–4th stages with d_{pa50} smaller than 260 nm was not measured.

Another practical problem needs to be addressed is particle clogging in the nozzles due to long-term or high particle concentration sampling, which may often be ignored by many users since this problem develops slowly. The clogged nozzles may result in an increase in the pressure drop across the cascade impactor and eventually a decrease in the d_{pa50} values of the lower stages (Ji et al., 2006). Therefore, dirty nozzle plates need to be cleaned regularly. For the lower 7th–10th stages of the MOUDI, the nozzles may be clogged easily due to its step-shaped structure with abrupt contraction, as shown in Fig. 1a–c, in which the cross sectional view, top views at the depth of 0 μm and 150 μm, respectively, are shown for the 9th stage nozzle of the MOUDI as an example (MSP Model 110). The larger dashed circle in Fig. 1c shows the circumference of the step before the nozzle hole where particles may deposit easily resulting in possible nozzle clogging. In addition, since the bottom part of the nozzle used to determine the nozzle diameter is thin and fragile, cleaning by ultra-sonication is not recommended for fear that possible nozzle fracture may occur (MSP, 2006). Otherwise, ultra-sonication is an effective way to dislodge particles deposited in the nozzle.

In this study, the original 7th–10th stages in one of the MOUDI were replaced by the new nozzle plates with smooth nozzle shape fabricated by the LIGA process (Lithography, Electroplating, and Molding). The cascade impactor is hereafter referred to as the NMCI (NCTU micro-orifice cascade impactor). The cross sectional view, top views at the depth of 0 μm and 120 μm of the new nozzle can be seen in Fig. 1e–g. Furthermore, the bottom views of the nozzle of the MOUDI and the NMCI shown in Fig. 1d and h, respectively, indicate that the latter is closer to a perfect round shape than the former. In the laboratory, the particle collection efficiency curves of the 7th–10th stages of the NMCI and those of the MOUDI were obtained to ensure d_{pa50} values match with the nominal values given in Marple et al. (1991). After that, the total interstage loss of nanoparticles from the inlet to each lower stage (7th–10th) of both NMCI and MOUDI was measured. The comparison test of the collocated NMCI and MOUDI was also conducted in two ambient air monitoring stations. Finally, to examine if nozzle clogging occurs in both cascade impactors, the pressure drop across the inlet to the 9th stage of the cascade impactors was monitored during sampling of high concentration incense smokes. After the test, nozzle was examined under a microscope for possible nozzle clogging.

2. Experiment methods

The experimental setup for measuring particle collection efficiency and nanoparticles loss is shown in Fig. 2. Monodisperse liquid dioctyl sebacate (DOS) particles with the aerodynamic diameter (d_{pa}) from 15 to 500 nm were generated by the atomization and electrostatic classifier technique for the test. Polydisperse particles were first generated by the constant output atomizer (TSI Model 3076) from the DOS solution with the concentration from 0.001 to 0.1 % (v/v). The aerosol flow was passed through a tubular furnace (Lindberg/Blue, Model HTF55322C, USA) at a fixed temperature of 300 °C to produce a relatively narrow size distribution by the evaporation-condensation process. Monodisperse, singly charged particles were then generated by the electrostatic classifier (EC, TSI Model 3080) equipped with the nano-differential mobility analyzer (DMA, TSI Model 3085) or the long-DMA (TSI Model 3081). To minimize the effect of multiple charges on the monodispersity of the classified particles (Pui and Liu, 1979), only particles larger than the count median diameter (CMD) were classified. When calibrating the particle collection efficiency of a single lower stage, a ball valve was used to simulate the pressure drop created by all previous upstream stages. The following equation was then used to calculate the particle collection efficiency (η) or interstage loss (L) as:

$$\eta \text{ or } L = \left(1 - \frac{I_2}{I_1}\right) \times 100 \quad (1)$$

where the I_1 and I_2 are the aerosol currents at the inlet or outlet of the tested impactors measured by the TSI 3068 aerosol electrometer (AE) equipped with a home-made faraday gage which is similar to that in the original TSI AE except that a larger tube for the aerosol flow (inner diameter is 7.3 mm compared to 3.1 mm of the original one) is used inside it to reduce the pressure drop.

After the laboratory tests, field comparison and nozzle clogging tests were conducted. For the field comparison test, the NMCI and the MOUDI were collocated to measure ambient aerosol mass size distributions at the Jhongshan and Jhudong air monitoring stations, Taiwan. These two sampling sites were chosen because they are ideal urban sites with typical bimodal mass size distributions, where the distances from the stations to the nearest main road are 15 and 300 m for the Jhongshan and Jhudong stations, respectively. Silicone grease (KF-96-SP, Topco Technologies Corp., Taiwan) coated aluminum foils were used as the impaction substrates in the 0th–10th stages to reduce solid particle bounce, and Teflon filters (Zefluor P5PJ047, Pall Corp., New York, USA) were used as the after filter. Before weighing, the substrates were conditioned in an environmental conditioning room where the RH and temperature were kept at 40 ± 2% and 21 ± 1 °C, respectively. A microbalance (Model CP2P-F, Sartorius, Germany) was used for weighing, in

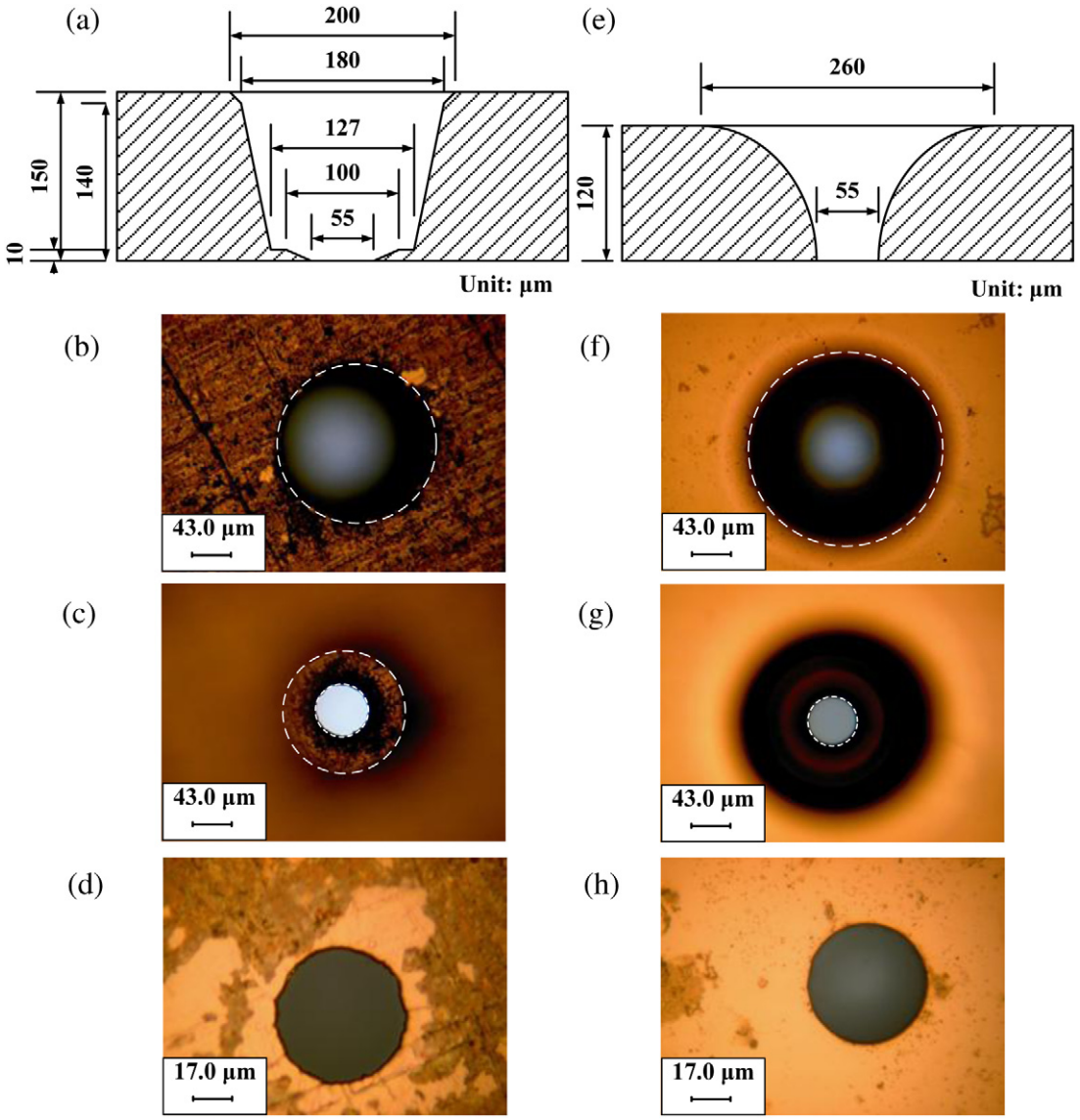

Fig. 1. (a) Cross-section view, front view at (b) depth = 0 and (c) 150 μm, and (d) back view of a 9th stage nozzle of the MOUDI; (e) cross-section view, front view at (f) depth = 0 and (g) 120 μm, and (h) back view of a 9th stage nozzle of the NMCI. (Dashed circles demarcate the circumferences of the step or holes).

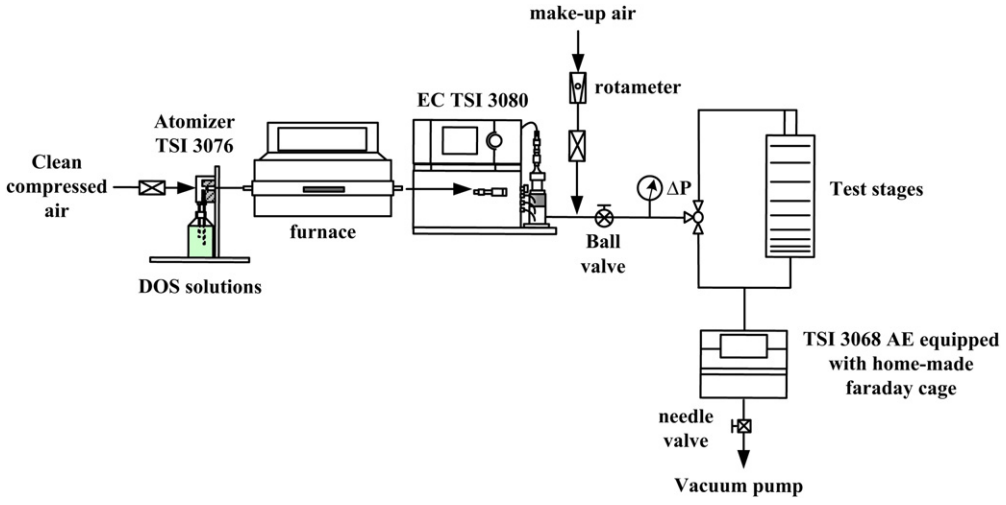

Fig. 2. Experimental setup to measure the particle collection efficiency and nanoparticle loss.

which the electrostatic charge of the Teflon filters were neutralized by an ionizing air blower (Model CSD-0911, MEISEI, Japan).

To examine possible nozzle clogging, the pressure drop of the NMCI and the MOUDI was monitored continuously during sampling of high concentration (25 mg m^{-3}) incense smokes with the mass median aerodynamic diameter (MMAD) of 500 nm for 45 min. The reason for sampling with incense smokes instead of ambient aerosols is to provide about 1000 times higher submicron particle and nanoparticle concentrations than those of ambient aerosols for testing the lower 7th–10th stages of the cascade impactors to save testing time, which would otherwise be too long to conduct the tests. After sampling, dirty nozzle plates were observed under an optical microscopy (ESPA, Model IM35) for possible nozzle clogging.

3. Results and discussion

3.1. Particle collection efficiency curves

Fig. 3 shows the calibrated particle collection efficiency curves of the 7th–10th stage of the NMCI and those of the MOUDI. The calibration results together with the design parameters are summarized in Table 1. It shows that after adjusting proper S/W ratios (S: jet to plate distance; W: nozzle diameter), the d_{pa50} values of the 7th–10th stage of the NMCI and those of the MOUDI are close to the nominal values, which are 320, 180, 100 and 56 nm, respectively, given in Marple et al. (1991). The S/W ratio of the 9th stage of the NMCI, 13.44, is very close to that of the micro-orifice impactor in the PENS (personal nanoparticle sampler) in which d_{pa50} is 100 nm and S/W is 13.8 (Tsai et al., 2012).

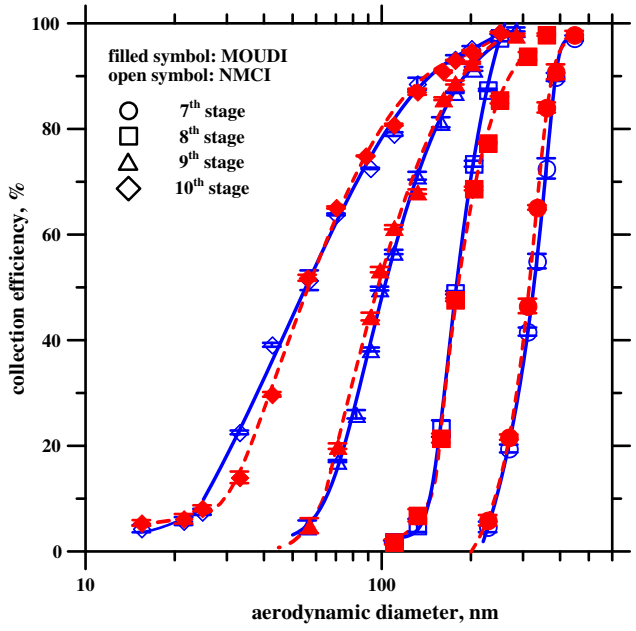

Fig. 3. Particle collection efficiency curves of the 7th–10th stages of the MOUDI and NMCI.

From Table 1, it can also be seen that the S/W ratios of the 7th and 8th MOUDI stages, which are 5.56 and 11.32, respectively, are larger than those of the NMCI, which are 2.52 and 3.01, respectively. This is because that the nozzle diameters of the former are smaller than the latter. Conversely, the S/W ratios of the 9th and 10th MOUDI stages, which are 9.3 and 10.9, respectively, are smaller than those of the NMCI, which are 13.44 and 24.75, respectively, because the corresponding nozzle diameters of the former are larger than the latter. Besides the difference in the nozzle diameter, partial particle clogging in the 7th and 8th stages of the MOUDI after it has been used for more than 5 years despite its regular nozzle cleaning may also explain why different S/W ratios are needed to maintain the correct d_{pa50} values. Smaller nozzle diameter in the 10th NMCI stage also leads to a larger pressure drop and a larger S/W ratio is needed to maintain the d_{pa50} of 56 nm as compared to the MOUDI. Similar sensitive S/W effect on the cutoff diameters was also found in the PENS (Tsai et al., 2012), which deserves future study to facilitate the design of the micro-orifice cascade impactor.

The above calibration results are for the individual stages of the two cascade impactors. When the upstream stages are present, the total collection efficiency curves form the inlet to one of the lower stages is shown in Fig. 4. The left tail ends of the total collection efficiency curves are seen to lift upward when the upstream stages are present due to the convectional diffusion of nanoparticles in the stages. Similar results were also found in previous studies (Marple et al., 1991; Tsai et al., 2012). It can also be observed that for the inlet to the 9th or 10th stage, there is a shift of the collection efficiency curve to the left (i.e. to the smaller particle size) as compared to that calibrated individually, and the corresponding d_{pa50} is decreased from 102 to 92.4 nm or 55.7 to 47.1 nm, respectively.

An additional check was also made by estimating the total collection efficiency from the inlet to the 9th stage ($\eta^*_{T,9}$) or to the 10th stage ($\eta^*_{T,10}$) using the following equation:

$$\eta^*_{T,i} = 1 - (1 - \eta_{T,i-1})(1 - \eta_i) \quad (2)$$

where $\eta_{T,i}$ and η_i are the total collection efficiency of the inlet to the ith stage and the collection efficiency of the individual ith stage, respectively. Results are plotted as filled symbols in Fig. 4 in which $\eta^*_{T,10}$ and $\eta^*_{T,9}$ are shown to agree well with those of the experimental total collection efficiencies with the average absolute relative difference of 3.2 and 4.2%, respectively. For the 8th stage, however, such a shift in the collection efficiency curve is not observed. This is because that partial overlapping of the lower part of the collection efficiency curve of the 8th or 9th stage with the upper part of the collection curve of the 9th or 10th stage occurs. In addition, the total collection efficiency curves of the inlet to the 9th and 10th stage are affected by convectional diffusion deposition of nanoparticles in all previous stages, which is only important for

Table 1
Summary of the calibration results and the design parameters of the 7th–10th stage of the NMCI and the MOUDI.

Stage	Marple et al. (1991)				MOUDI				NMCI			
	Nominal d_{pa50} (nm)	Nozzle dia. (μm)	[a]S/W	[b]P/P_0	d_{pa50} (nm)	Nozzle dia. (μm)	[a]S/W	[b]P/P_0	d_{pa50} (nm)	Nozzle dia. (μm)	[a]S/W	[b]P/P_0
7	320	140	4.1	0.95	314.4	135	5.56	0.95	323	138.7	2.52	0.95
8	180	90	6.4	0.89	180.8	102	11.18	0.87	178.5	109.5	3.01	0.89
9	100	55	10.6	0.76	97.0	57	9.30	0.72	102	54.3	13.44	0.72
10	56	52	11.1	0.53	56.5	52.3	10.90	0.47	55.7	50.9	24.75	0.34

[a] S = jet to plate distance, W = nozzle diameter.
[b] P = absolute pressure at stage exit with all upstream stages in place, P_0 = ambient pressure.

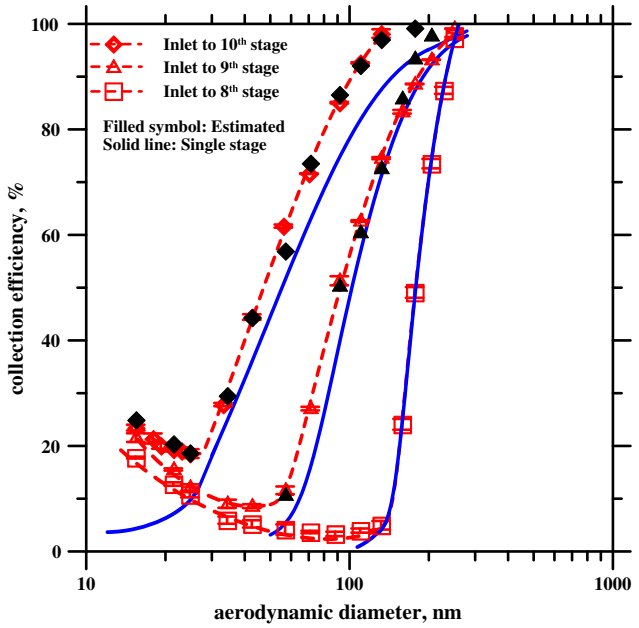

Fig. 4. Particle collection efficiency curves of the 8th–10th stage of the NMCI with all upstream stages in place.

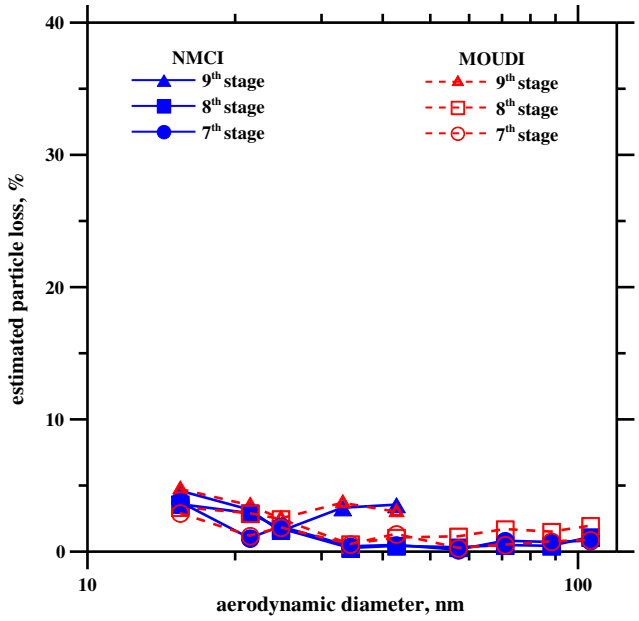

Fig. 6. Estimated single stage nanoparticle loss in the 7th–9th stage of the MOUDI and NMCI.

nanoparticles, or particles with d_{pa} less than 100 nm. Therefore, in order to obtain more accurate size resolution of nanoparticles, nanoparticle loss of all upstream stages should also be considered.

3.2. Interstage loss of nanoparticles

Fig. 5 shows the total interstage loss of nanoparticles from the inlet to each of the lower stages of the NMCI and those of the MOUDI. It is noted that in order to distinguish the interstage loss of nanoparticles from the collection efficiency of the 9th and 10th stages, only particles with d_{pa} near the lower end of the collection efficiency curve where $d_{pa} < d_{pa50}$ were used for the tests, which

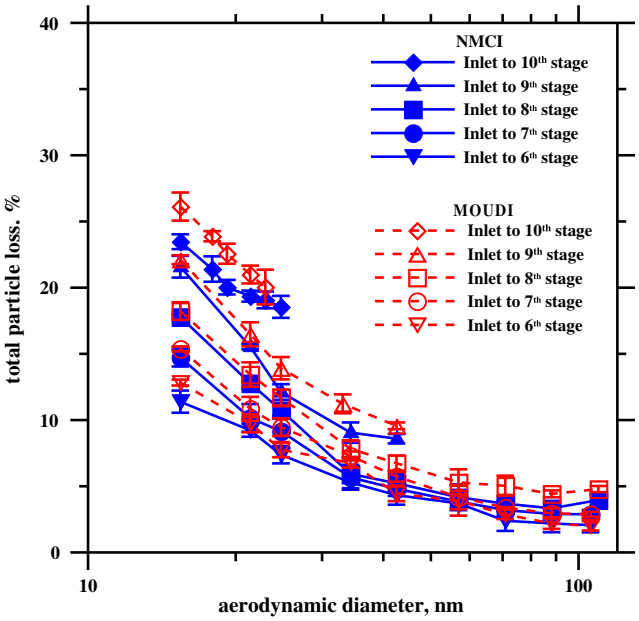

Fig. 5. Total interstage loss of nanoparticles from the inlet to different stages of the MOUDI and NMCI.

were 15.4–42.5 and 15.4–25 nm, respectively. For other stages, nanoparticles with d_{pa} from 15.4 to 105 nm were used. Results show that total nanoparticle loss increases with decreasing d_{pa} due to convectional diffusion deposition. The maximum loss from the inlet to the 6th–10th stage occurs at d_{pa} of 15.4 nm, which is 11.39–23.47 % for the NMCI, and 12.83–26.13 % for the MOUDI. The total interstage loss of nanoparticles in the NMCI is slightly lower than those in the MOUDI due to smoother nozzle shape of the former. For both impactors, a significant total interstage loss of nanoparticles from the inlet to one of the lower stages (7th–10th) exists especially for nanoparticles with the diameter smaller than 40 nm. For nanoparticles larger than 40 nm, the total interstage loss is less than 10% and it decreases with increasing particle diameter. It is therefore important to consider the nanoparticle loss in the 10th stage when determining the mass distributions of nanoparticles.

In order to determine how much loss exists in each single stage, the following equation is used:

$$L_i^* = \frac{L_{T,i} - L_{T,i-1}}{1 - L_{T,i-1}} \quad (3)$$

where L_i^* is the estimated single stage loss in the ith stage, and $L_{T,i}$ is the experimental total interstage loss from inlet to the ith stage. The L_7^* to L_9^* of the NMCI and those of the MOUDI are shown in Fig. 6 where it shows the loss is below 5% for each single stage and is gradually increased with decreasing d_{pa} due to convectional diffusion deposition. This small particle loss per individual stage prevents accurate loss measurement as stated in the previous section. The maximum L_7^* to L_9^* occur at d_{pa} of 15.4 nm, which are 3.59–4.61 % and 2.93–4.74 %, for the NMCI and the MOUDI, respectively. The loss L_0^*–L_6^* is estimated to be small, which is less than 1.6 and 1.8%, if the total loss $L_{T,6}$ of 11.39 and 12.83% is assumed to be evenly divided in the inlet to 6th stages for the NMCI and the MOUDI, respectively.

3.3. Field comparison and nozzle clogging test

The ambient mass size distributions measured by the NMCI and those by the collocated MOUDI are shown in Fig. 7. The mass size

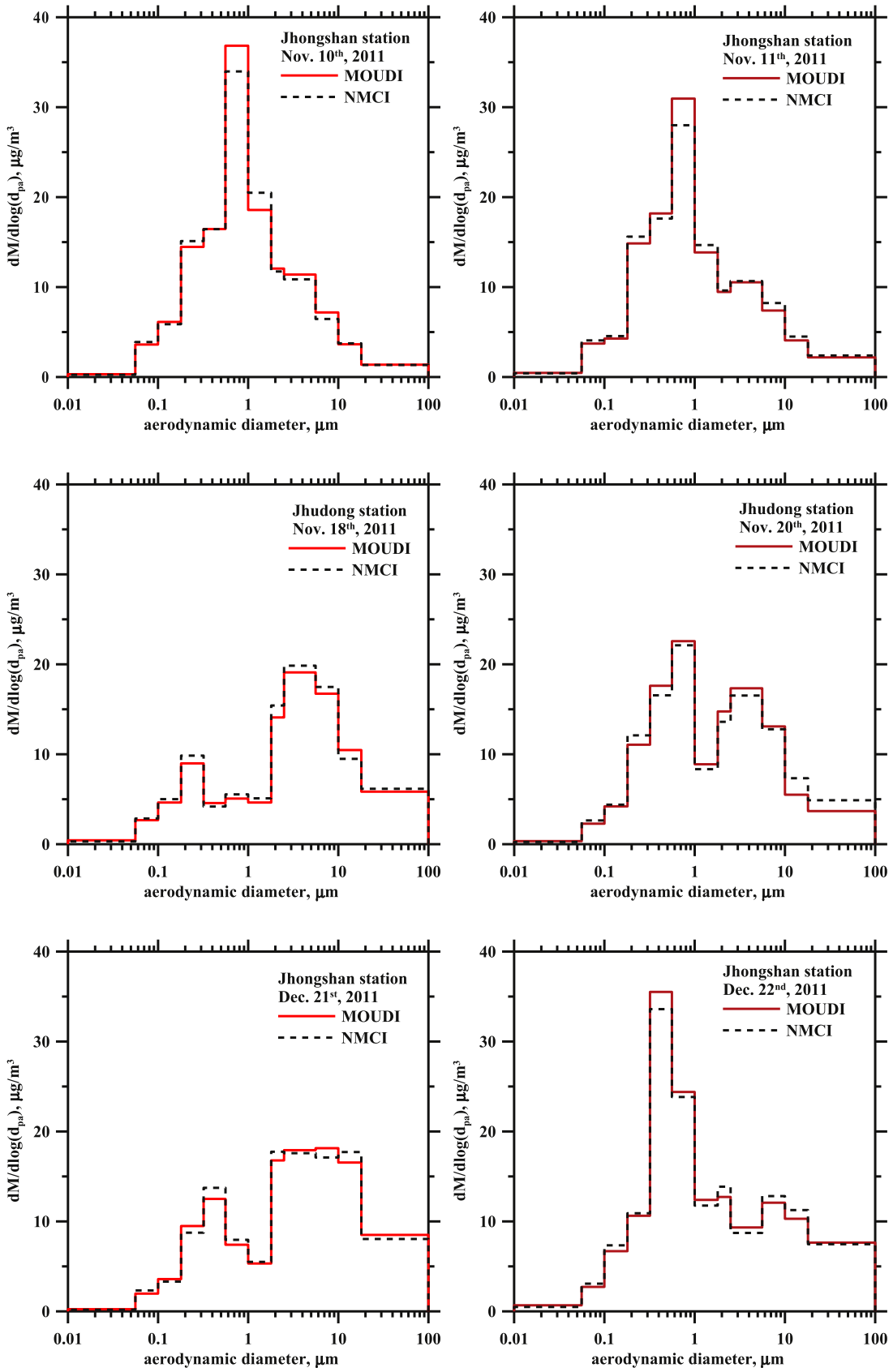

Fig. 7. Ambient aerosol mass size distributions measured by the NMCI and the collocated MOUDI.

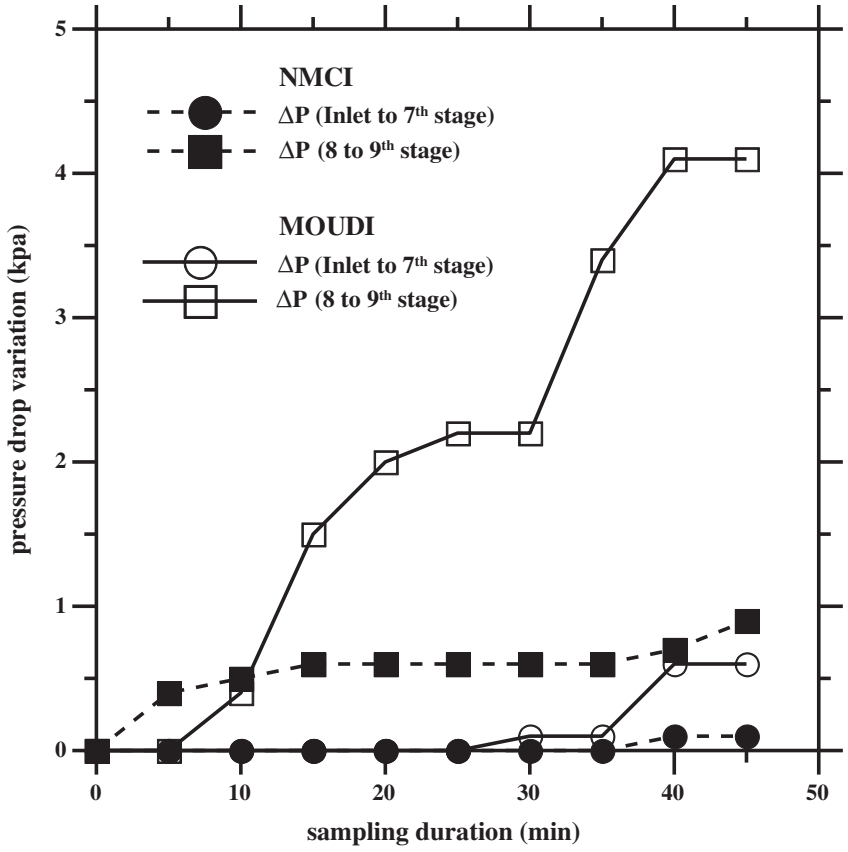

Fig. 8. Variation of pressure drop in the MOUDI and the NMCI during sampling of high concentration (25 mg m^{-3}) incense smokes for 45 min.

distributions measured by the NMCI are seen to be very close to those by the MOUDI. The mass concentration data of all stages of these two cascade impactors have the relative difference of less than 10%, except the final stage where the concentrations of the NMCI is 9.6–27.3 % (average 23.4 ± 7%) lower than those of the MOUDI. This is possibly due to more evaporation of semi-volatile components in the NMCI since its final stage is at a lower pressure condition than the MOUDI.

Fig. 8 shows the results of nozzle clogging test expressed in terms of the variation of pressure drop (△ P) across the inlet to 7th

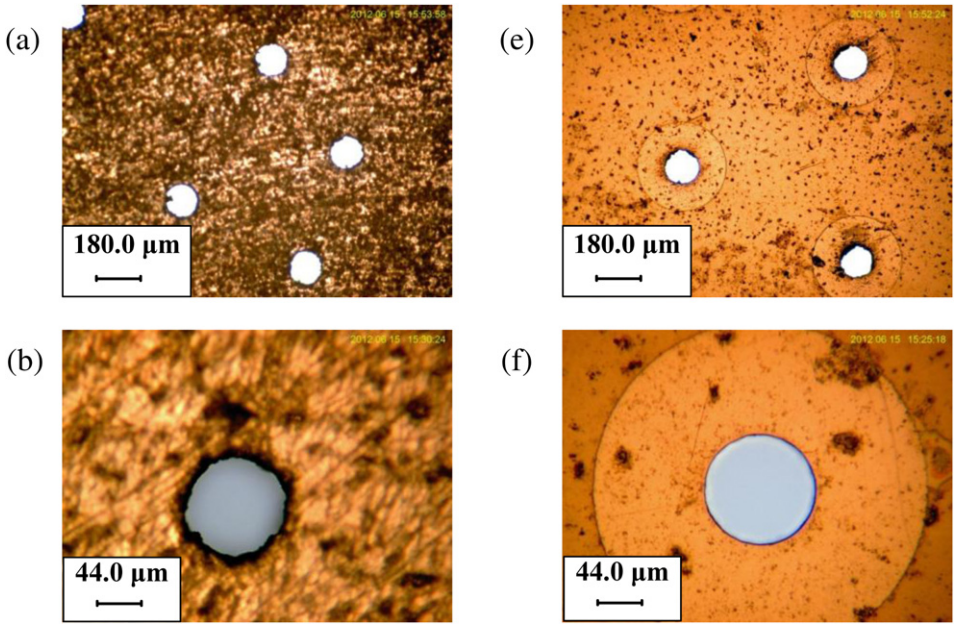

Fig. 9. Micrograph of the 7th–10th [(a) to (d)] stage nozzles of the MOUDI and the 7th–10th [(e) to (h)] stage nozzles of the NMCI after incense smoke sampling.

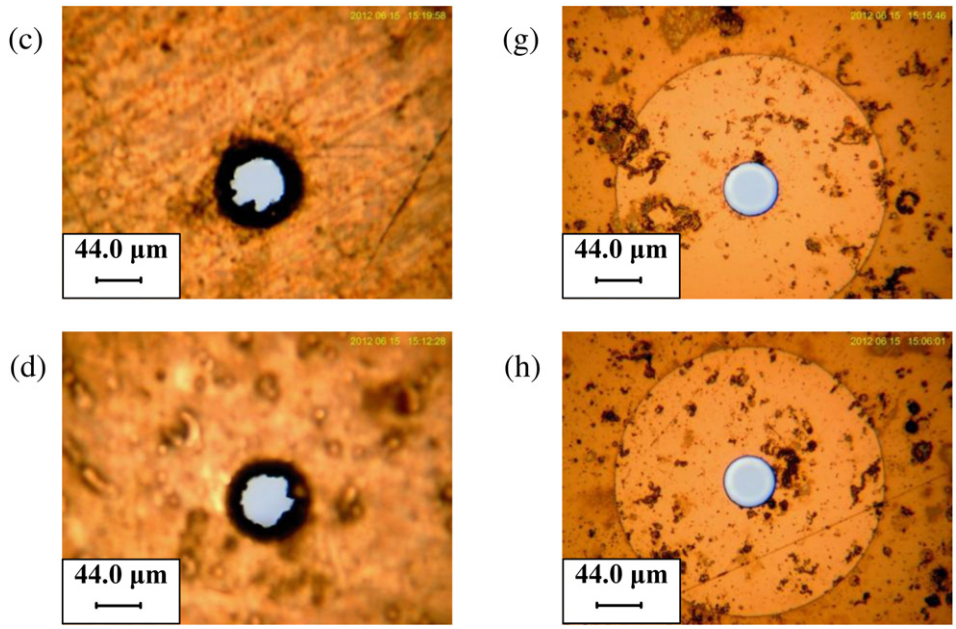

Fig. 9. (*Continued*)

or the 8th–9th stage of the NMCI and the MOUDI during sampling of high concentration incense smokes for 45 min. It can be clearly seen that $\triangle P$ increase in the MOUDI is significantly higher than that of the NMCI across the 8th–9th stage. That means particle clogging in the 8th and 9th stage nozzles of the former is more severe than those of the latter. Micrographs shown in Fig. 9 provide further evidence of nozzle clogging in the 7th–10th stages of the MOUDI while it is much less severe in the NMCI. That is, the new nozzle plates in the lower stages of the NMCI outperform those of the MOUDI in preventing nozzle clogging.

4. Conclusions

In this study, new nozzle plates with smooth shaped nozzles were fabricated by the LIGA process in order to avoid possible particle clogging in the nozzles. The micro-orifice cascade impactor using the new nozzle plates in the 7th–10th stages (NMCI) and the MOUDI were studied for the particle collection efficiency and nanoparticle interstage loss. In addition, field comparison and nozzle clogging tests were conducted.

Calibration results show that after adjusting the S/W ratios to proper values, the d_{pa50} of the 7th–10th stage of the NMCI and those of the MOUDI are very close to the nominal values given in Marple et al. (1991). It is also found that the d_{pa50} of the nanoparticle stages (9th and 10th) of the MOUDI obtained from the single stage calibration will decrease by 9.4 and 15.4%, respectively, if all upstream stages are present.

For both impactors, a significant total interstage loss of nanoparticles from inlet to one of the lower stages (7th–10th) exists especially for nanoparticles with d_{pa} smaller than 40 nm. For nanoparticles larger than 40 nm, the total interstage loss is less than 10% and it decreases with increasing particle diameter. It is therefore important to consider the nanoparticle loss in the 10th stage of the cascade impactors when determining the mass distributions of nanoparticles. If the size distribution of nanoparticles smaller than 56 nm is to be determined by using the instrument such as the 13-stage MOUDI-II (MSP, Model 122 or 125), nanoparticle loss in the stages 11–13 is expected to be even more severe and warrants further investigation.

Field sampling results show that the mass size distributions measured by the NMCI agree well with those of the MOUDI. The nozzle clogging test further indicates that the NMCI outperforms the MOUDI in preventing possible nozzle clogging. In addition, the present NMCI has a sturdy nozzle structure, which allows ultrasonication of the plates for better cleaning efficiency to remove deposited particles in the nozzles. It is expected that the NMCI can facilitate the accurate size-classified measurements of nanoparticles in the future.

Acknowledgments

The authors would like to express the gratitude to the Taiwan National Science Council for financial support under contract (NSC 98-2221-E-009-020-MY3) and the Taiwan Environmental Protection Agency under contract (EPA-100-1602-02-01).

References

Chang, M., Kim, S., Sioutas, C., 1999. Experimental studies on particle impaction and bounce: effects of substrate design and material. Atmospheric Environment 33, 2313–2322.

Chen, S.C., Tsai, C.J., Chou, C.C.K., Roam, G.D., Cheng, S.S., Wang, Y.N., 2010. Ultrafine particles at three different sampling locations in Taiwan. Atmospheric Environment 44, 533–540.

Chen, S.C., Tsai, C.J., Chen, H.D., Huang, C.Y., Roam, G.D., 2011. The influence of relative humidity on nanoparticle concentration and particle mass distribution measurements by the MOUDI. Aerosol Science and Technology 45, 596–603.

Chow, J.C., Watson, J.G., 2007. Review of measurement methods and compositions for ultrafine particles. Aerosol and Air Quality Research 7, 121–173.

Furuuchi, M., Eryu, K., Nagura, M., Hata, M., Kato, T., Tajima, N., Sekiguchi, K., Ehara, K., Seto, T., Otani, Y., 2010. Development and performance evaluation of air sampler with inertial filter for nanopartilce sampling. Aerosol and Air Quality Research 10, 185–192.

Hering, S.V., Flagan, R.C., Friedlander, S.K., Collins, J.J., Richards, L.W., 1979. Design and evaluation of new low-pressure impactor II. Environmental Science and Technology 13, 184–188.

Hillamo, R.E., Kauppinen, E.I., 1991. On the performance of the Berner low pressure impactor. Aerosol Science and Technology 14, 33–47.

Huang, C.H., Tsai, C.J., Shih, T.S., 2001. Particle collection efficiency of an impactor with porous metal substrates. Journal of Aerosol Science 32, 1035–1044.

Huang, C.H., Chang, C.S., Chang, S.H., Tsai, C.J., Shih, T.S., Tang, D.T., 2005. Use of porous foam as the substrate of an impactor for respirable aerosol sampling. Journal of Aerosol Science 36, 1373–1386.

Ji, J.H., Bae, G.N., Hwang, J., 2006. Observation and evaluation of nozzle clogging in a micro-orifice impactor used for atmospheric aerosol sampling. Particulate Science and Technology 24, 85–96.
Keskinen, J., Pietarinen, K., Lehtimaki, M., 1992. Electrical low pressure impactor. Journal of Aerosol Science 23, 353–360.
Kim, P.R., Han, Y.J., Holsen, T.M., Yi, S.M., 2012. Atmospheric particulate mercury: concentration and size distributions. Atmospheric Environment 61, 94–102.
Kudo, S., Sekiguchi, K., Kim, K.H., Kinoshita, M., Möller, D., Wang, Q., Yoshikado, H., Sakamoto, K., 2012. Differences of chemical species and their ratios between fine and ultrafine particles in the roadside environment. Atmospheric Environment 62, 172–179.
Liu, C.N., Chen, S.C., Tsai, C.J., 2011. A novel multi-filter PM_{10}–$PM_{2.5}$ sampler (MFPPS). Aerosol Science and Technology 45, 1480–1487.
Marple, V.A., Rubow, K.L., Behm, S.M., 1991. A microorifice uniform deposit impactor (MOUDI): description, calibration and use. Aerosol Science and Technology 14, 434–446.
Marple, V.A., Rubow, K.L., Olson, B.A., 2001. Inertial, gravitational, centrifugal, and thermal collection techniques. In: Baron, P.A., Willeke, K. (Eds.), Aerosol Measurement: Principles, Techniques and Applications. Wiley Interscience, New York, pp. 229–260.
MSP Corporation, 2006. Model 100/110 MOUDI™ User Guide (Shoreview, Minnesota).
Otani, Y., Eryu, K., Furuuchi, M., Tajima, N., Tekasakul, P., 2007. Inertial classification of nanoparticles with fibrous filters. Aerosol and Air Quality Research 7, 343–352.
Pak, S.S., Liu, B.Y.H., Rubow, K.L., 1992. Effect of coating thickness on particle bounce in inertial impactors. Aerosol Science and Technology 16, 141–150.
Peters, T.M., Vanderpool, R.W., Wiener, R.W., 2001. Design and calibration of the EPA $PM_{2.5}$ well impactor ninety-six (WINS). Aerosol Science and Technology 34, 389–397.
Pui, D.Y.H., Liu, B.Y.H., 1979. Electrical aerosol analyzer: calibration and performance. In: Lundgren, D.A., et al. (Eds.), Aerosol Measurement. University of Florida Press, Gainesville, Florida, pp. 384–399.
Tsai, C.J., Cheng, Y.H., 1995. Solid particle collection characteristics on impaction surfaces of different designs. Aerosol Science and Technology 23, 96–106.
Tsai, C.J., Liu, C.N., Hung, S.M., Chen, S.C., Uang, S.N., Cheng, Y.S., Zhou, Y., 2012. Novel active personal nanoparticle sampler for the exposure assessment of nanoparticles in workplaces. Environmental Science and Technology 46, 4546–4552.
Turner, J.R., Hering, S.V., 1987. Greased and oiled substrates as bounce-free impaction surfaces. Journal of Aerosol Science 18, 215–224.
Vasiliou, J.G., Sorensen, D., McMurry, P.H., 1999. Sampling at controlled relative humidity with a cascade impactor. Atmospheric Environment 33, 1049–1056.
Virtanen, A., Marjamäki, M., Ristimäki, J., Keskinen, J., 2001. Fine particle losses in electrical low-pressure impactor. Journal of Aerosol Science 32, 389–401.
Wang, S., Wei, W., Li, D., Aunan, K., Hao, J., 2010. Air pollutants in rural homes in Guishou, China-concentration speciation, and size distribution. Atmospheric Environment 44, 4575–4581.
Zhu, C.S., Chen, C.C., Cao, J.J., Tsai, C.J., Chou, C.C.K., Liu, S.C., Roam, G.D., 2010. Characterization of carbon fractions for atmospheric fine particles and nanoparticles in a highway tunnel. Atmospheric Environment 44, 2668–2673.
Zhu, C.S., Tsai, C.J., Chen, S.C., Cao, J.J., Roam, G.D., 2012. Positive sampling artifacts of organic carbon fractions for fine particles and nanoparticles in a tunnel environment. Atmospheric Environment 54, 225–230.